Available online at www.sciencedirect.com
SCIENCE DIRECT®
International Journal of Mass Spectrometry 228 (2003) 221–235
International Journal of Mass Spectrometry
www.elsevier.com/locate/ijms

# Sequential bond energies of $Ag^+(H_2O)_n$ and $Ag^+$(dimethyl ether)$_n$, $n = 1$–4, determined by threshold collision-induced dissociation

Hideya Koizumi, Melissa Larson, Felician Muntean, P.B. Armentrout*

*Department of Chemistry, University of Utah, Salt Lake City, UT 84112, USA*

Received 2 December 2002; accepted 17 March 2003

In celebration of Helmut Schwarz's 60th birthday, in appreciation of his unique contributions to ion–molecule chemistry, and in thanks for our collaborations.

**Abstract**

Collision-induced dissociation (CID) of the $Ag^+(H_2O)_n$ and $Ag^+$(dimethyl ether)$_n$ complexes for $n = 1$–4 is studied using kinetic energy-dependent guided ion beam mass spectrometry. In all cases, the primary products are endothermic loss of an intact neutral ligand from the complex. The cross-section thresholds are interpreted to yield 0 and 298 K bond energies after accounting for the effects of multiple ion–molecule collisions, internal energy of the complexes, and unimolecular decay rates. These values are compared favorably with previous experimental values for the water complexes and with ab initio theoretical values for all eight complexes. Our results are also compared with the analogous copper and alkali metal ion complexes, previously studied. Although $Ag^+$ and $Cu^+$ both have $^1S$ ($3d^{10}$) ground state electronic configurations, the comparison shows different trends for $Ag^+$ because of its larger ionic size.


*Keywords:* Guided ion beams; Thermochemistry; Silver ions; Dimethyl ether; Water; Solvation; Bond energies

## 1. Introduction

Noncovalent complexes of various metal ions are important in biological systems [1] and in advanced chemical separations [2] and analytical methodology [3]. Elucidation of such interactions can profitably be made by studying gas phase systems, which can provide fundamental and quantitative insight into the details of the interactions involved. Previously, we have examined noncovalent interactions between the simple monodentate ligands, water and dimethyl ether (DME), with alkali metal ions [4–9] and copper ions [10,11]. The alkali metal ions have spherically symmetric $^1S$ electronic ground states, as do singly charged ions of the coinage metals. However, the metal–ligand interactions, which can be described as mostly electrostatic, are stronger for coinage ion water clusters compared to alkali metal water clusters, as several groups have reported [12–14]. Bauschlicher et al. investigated $Cu^+$ water clusters using restricted Hartree–Fock (RHF) and modified coupled-pair functional (MCPF) theories [13]. Recently, Feller et al.

* Corresponding author. Tel.: +1-801-581-7885; fax: +1-801-581-8433.
*E-mail address:* armentrout@chem.utah.edu (P.B. Armentrout).

1387-3806/$ – see front matter © 2003 Elsevier Science B.V. All rights reserved.
doi:10.1016/S1387-3806(03)00211-2

studied coinage metal cation water and DME clusters using complete basis set coupled cluster techniques [14,15]. The results of these calculations are in good agreement with the experimental results [10–12] for most species, although somewhat poorer agreement was reported for $Cu^+(H_2O)_2$ and $Cu^+(DME)_n$ complexes for $n = 1$ and 2.

Comparable experimental studies on the silver ion are less complete. Sequential bond energies of $Ag^+$ to as many as six water and five ammonia molecules have been measured using high pressure mass spectrometry by Holland and Castleman [12]. Relative energetics for the diadducts of $Ag^+$ with several small molecules have been measured using exchange equilibria by Deng and Kebarle [16] and placed on an absolute scale using the values for $Ag^+(H_2O)_2$ from Holland and Castleman. Siu and coworkers measured the bond energies of $Ag^+$ to water, methanol, ethanol, diethyl ether, acetone [17], and several organonitriles [18] by threshold collision-induced dissociation (TCID) in a triple quadrupole mass spectrometer. In our laboratory, the interactions between $Ag^+$ and $C_6H_6$ [19] and the sequential bond energies of $Ag^+(CO)_n$ ($n = 1$–4) complexes [20] have been studied using TCID in a guided ion beam tandem mass spectrometer. Most recently, we studied the interaction between silver ion and one to four methanol molecules in a combined experimental and theoretical investigation [21].

In this project, we investigate the binding of $Ag^+$ to one to four water ($H_2O$) and DME molecules. Guided ion beam mass spectrometry is used to measure the kinetic energy-dependent cross-sections for collision-induced dissociation (CID) with Xe. Analysis of these results provides absolute binding energies of these complexes after consideration of reactant energy distributions, effects of multiple collisions, and lifetime effects. These results are compared to theoretical results of Feller et al. [14,15]. The binding energies of these complexes are compared to analogous $Cu^+$ and $K^+$ complexes [7,10,11,22] to show how the size and electronic structure of the metal cation influences the metal–ligand interactions. Comparisons to the sequential bond energies of related ligands, such as methanol, are also made.

## 2. Experimental methods

For all reactions studied here, cross-sections are collected using a guided ion beam tandem mass spectrometer (GIBMS) described previously [23,24]. $Ag^+(L)_n$ complexes are produced in a dc discharge flow tube ion source [24]. At the front end of a meter long flow tube, a dc discharge in an ~10% mixture of Ar in He creates $Ar^+$ ions that sputter metal ions from a silver cathode. The overall pressure is about 0.5 Torr and typical operating conditions of the dc discharge are 1.3 kV and 20 mA. Water and DME molecules are introduced about 50 cm downstream of the source and attached to the silver ions by three-body condensation. While the complexes traverse the remainder of the flow tube, they are thermalized by undergoing $>10^4$ collisions with the bath gases. The assumption of efficient thermalization is reasonable, as suggested by previous work [10,25–27]. Under typical flow tube conditions, the intensities of the reactant ion beams for both ligands are $\sim 10^4$/s for the singly ligated complexes, slightly larger for doubly and triply ligated complexes ($2 \times 10^4$ to $5 \times 10^4$/s), and very small for quadruply ligated complexes (~3000/s for the water complex and ~1000/s for the DME complex).

These ions are extracted from the source, accelerated, and focused into a magnetic sector momentum analyzer for mass analysis. The mass-selected ions are slowed to a desired kinetic energy and focused into an rf octopole ion guide [28,29]. The guide passes through a static gas cell containing xenon gas, used in our CID studies for reasons described elsewhere [10,30]. After exiting the gas cell, the product and remaining reactant ions drift to the end of the octopole, where they are extracted and focused into a quadrupole mass filter for mass analysis. A secondary electron scintillation ion counter detects the mass-analyzed reactant and product ions. These signals are converted to absolute reaction cross-sections as described previously [23]. Absolute uncertainties in these cross-sections are estimated to be ±20%. The $Ag^+(DME)_4$ experiment was performed on a second GIBMS [31] having a larger magnetic sector that more easily handles this large mass. The energy dependence

of the cross-sections for this system obtained with both instruments are comparable, but the absolute magnitudes are clearly more correct for the data obtained on the instrument having the larger mass range.

Sharp features in observed cross-sections are broadened by thermal motion of the xenon gas and the distribution of ion energies. The distribution and absolute zero of the ion kinetic energies are measured using the octopole as a retarding potential analyzer [23]. The uncertainty in the absolute energy scale is ±0.05 eV (lab). Typical distributions are Gaussian with a full width at half maximum (fwhm) between 0.2 and 0.8 eV (lab). Kinetic energies in the laboratory frame are converted to ion energies in the center-of-mass (CM) frame by $E(\mathrm{CM}) = E(\mathrm{lab})m/(M + m)$, where $M$ and $m$ are ion and neutral reactant masses, respectively. All energies cited in this paper are in the CM frame except as noted.

## 3. Results

### 3.1. Experimental observations

#### 3.1.1. CID of $Ag^+(H_2O)_n$

Experimental cross-sections for the CID of $Ag^+(H_2O)_n$, $n$ = 1–4, complexes with xenon are shown in Fig. 1. The primary process for all complexes is the loss of a single $H_2O$ ligand in reaction 1.

$$Ag^+(H_2O)_n + Xe \rightarrow Ag^+(H_2O)_{n-1} + H_2O + Xe \quad (1)$$

Other products, such as those obtained from ligand exchange $Ag^+(H_2O)_{n-1}Xe$, were not observed for all $n$, presumably because the signals are just too weak to observe routinely. For $n = 1$, the $Ag^+$ ion product cross-section has an apparent threshold of about 1.0 eV and levels off with a maximum magnitude of about 7 Å$^2$. For $n = 2$, the $Ag^+(H_2O)$ ion product cross-section has an apparent threshold near 0.7 eV and levels off with a maximum magnitude of 20 Å$^2$. For $n = 3$, the $Ag^+(H_2O)_2$ primary product ion cross-section has an apparent threshold near 0.1 eV. Also, small amounts of an $Ag^+(H_2O)$ secondary product are observed with an apparent threshold near 1.5 eV and a maximum magnitude of 6 Å$^2$. No $Ag^+$ product ions are observed at any energy studied for any of the $n$ = 2–4 complexes. For $n = 4$, the $Ag^+(H_2O)_3$ cross-section has a finite value at 0 eV, reaches a maximum of 75 Å$^2$ at 0.8 eV, and gradually decreases in magnitude to 45 Å$^2$. As this primary product cross-section decreases, the $Ag^+(H_2O)_2$ product slowly rises to its maximum magnitude of 33 Å$^2$. The sum of these two cross-sections is nearly flat, consistent with the sequential loss of two ligands. No other products are observed at any energy studied.

#### 3.1.2. CID of $Ag^+(DME)_n$

Experimental cross-sections for the CID of $Ag^+(DME)_n$, $n$ = 1–4, complexes with xenon are shown in Fig. 2. In all cases, the primary process for all complexes is the loss of a single DME ligand in reaction 2.

$$Ag^+(DME)_n + Xe \rightarrow Ag^+(DME)_{n-1} + DME + Xe \quad (2)$$

For $n = 1$, the primary $Ag^+$ ion product cross-section has an apparent threshold of about 1.0 eV and levels off with a maximum magnitude of 12 Å$^2$. No other products are observed in any energy studied. For $n = 2$, the primary $Ag^+(DME)$ ion product cross-section has an apparent threshold near 0.5 eV and levels off with a maximum magnitude of 32 Å$^2$. The ligand exchange product ion, $Ag^+(DME)Xe$, has a similar apparent threshold and has its maximum of 0.8 Å$^2$ at 1.5 eV, decreasing slowly at higher energies. (Note that the sensitivity of this particular experiment is higher than for any of the other systems studied here, which probably accounts for why such ligand exchange products were only observed in this system.) This species decomposes by loss of the Xe ligand, as $Ag^+(Xe)$ is not observed. Small amounts (0.2 Å$^2$ maximum) of the $Ag^+$ secondary product are observed at higher energies starting near 2.6 eV. For $n = 3$, the $Ag^+(DME)_2$ primary product ion cross-section has an apparent threshold near 0 eV and rises sharply to a maximum of 85 Å$^2$ at 0.8 eV. Its magnitude gradually decreases to 70 Å$^2$ while the cross-section for the secondary

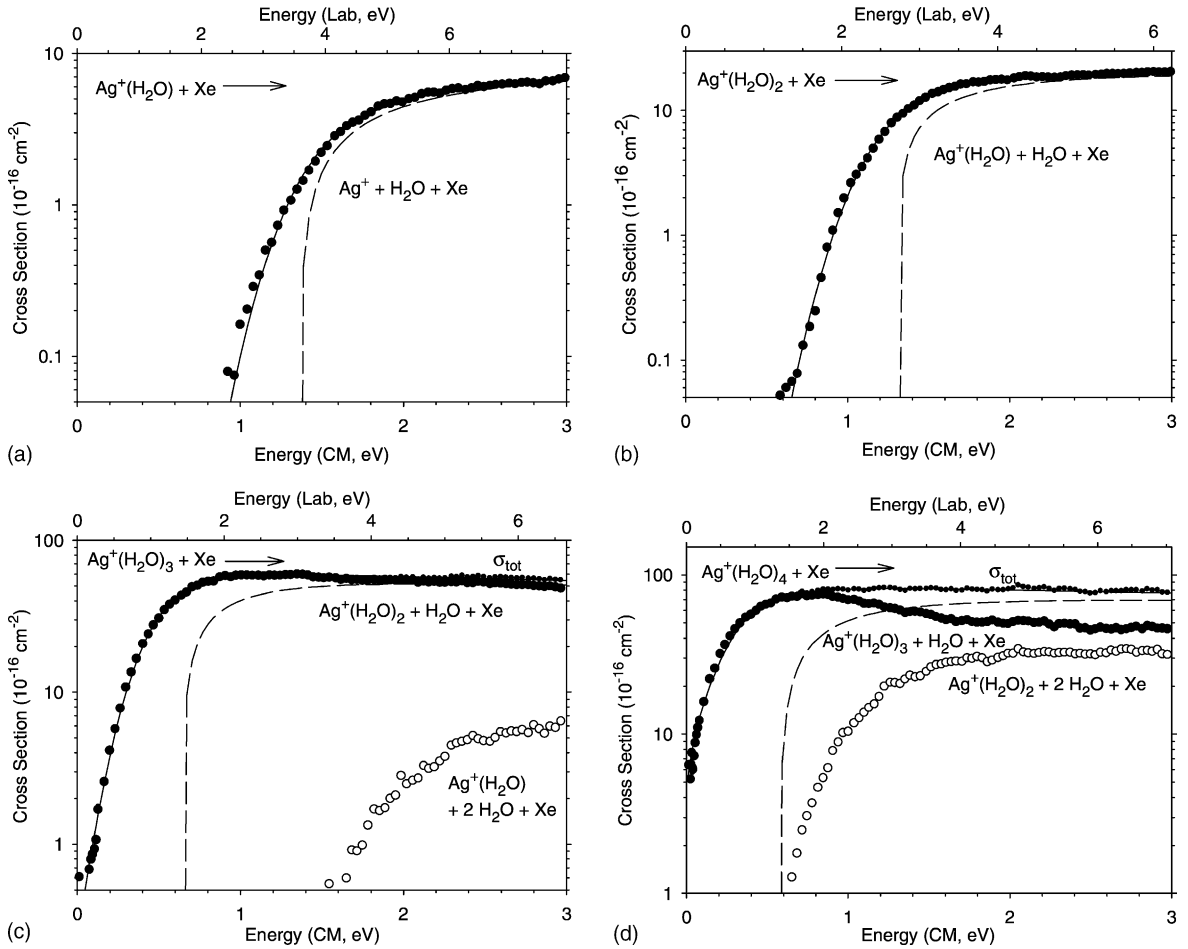


Fig. 1. Cross-sections for reactions of $Ag^+(H_2O)_n$ for $n = 1$–4 (parts a–d, respectively) with xenon as a function of kinetic energy in the center-of-mass frame (lower $x$ axis) and laboratory frame (upper $x$ axis). The dashed lines show the model of Eq. (3) for reactants with no internal energy and in the absence of kinetic energy broadening. Solid lines are from this model convoluted with the internal and kinetic energy distributions of the reactants. In parts c and d, the small circles show the total experimental cross-section.

$Ag^+$(DME) product ion rises to about 10 Å$^2$ at 3.6 eV from an apparent threshold of ~1.9 eV. No other ions are observed at any energy studied. For $n = 4$, the $Ag^+(DME)_3$ primary product ion cross-section has a large value at 0 eV and rises sharply to its maximum of 230 Å$^2$ at 0.8 eV. The cross-section for secondary $Ag^+(DME)_2$ product rises slowly from 0.4 eV and levels off at about 100 Å$^2$. The sum of these two product ion is relatively constant above 0.5 eV, consistent with sequential ligand loss. No other product ions are observed for this experiment.

### 3.2. Thermochemical and threshold analysis

The kinetic energy dependence of the experimental cross-sections is modeled using Eq. (3),

$$\sigma(E) = \frac{\sigma_0 \sum g_i (E + E_i - E_0)^N}{E} \quad (3)$$

where $E$ is the relative translational energy of the reactants, $E_0$ is the 0 K threshold of the reaction, $\sigma_0$ is an energy-independent scaling factor, and $N$ is an adjustable parameter that is related to the efficiencies of

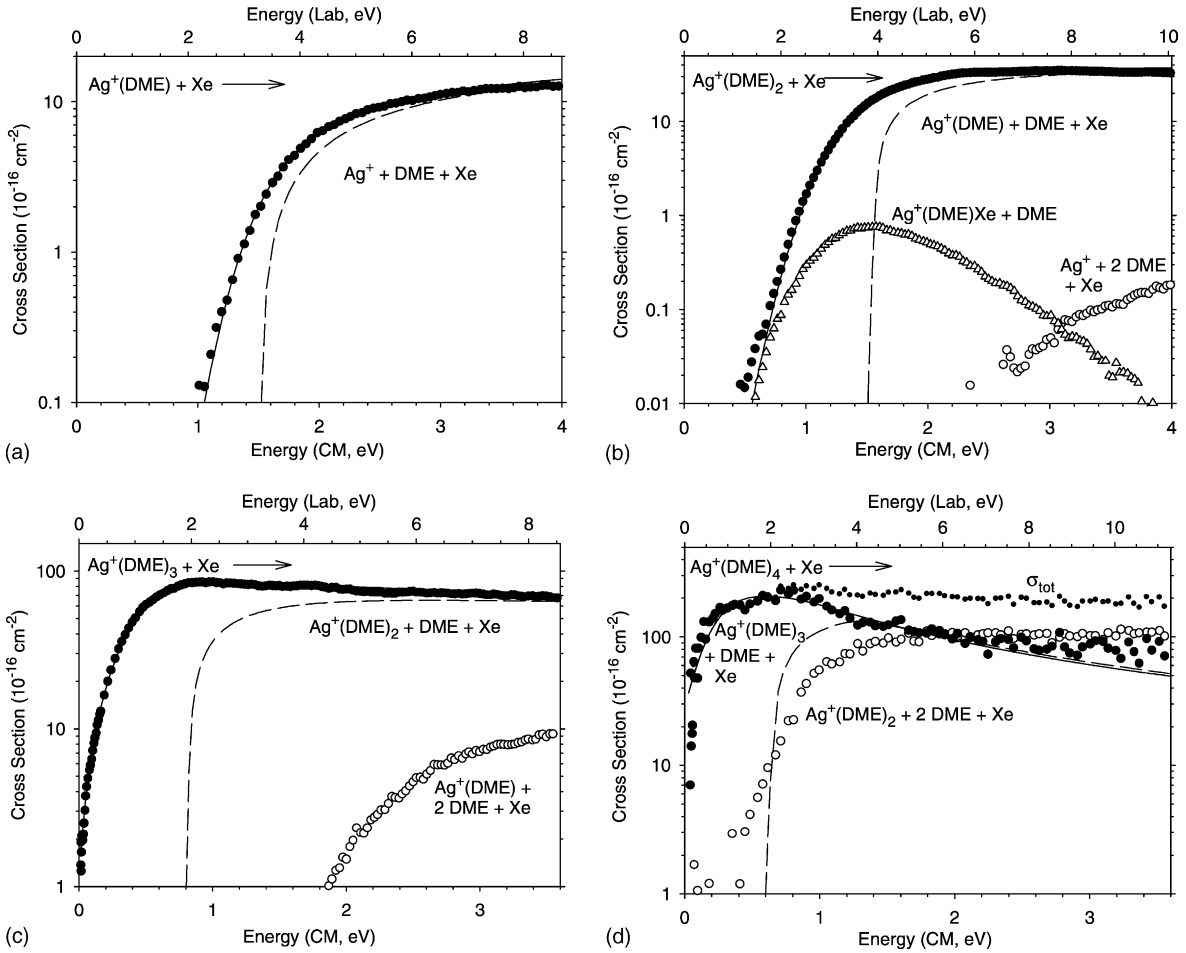


Fig. 2. Cross-sections for reactions of $Ag^+(DME)_n$ for $n = 1$–4 (parts a–d, respectively) with xenon as a function of kinetic energy in the center-of-mass frame (lower $x$ axis) and laboratory frame (upper $x$ axis). The dashed lines show the model of Eq. (3) for reactants with no internal energy and in the absence of kinetic energy broadening. Solid lines are from this model convoluted with the internal and kinetic energy distributions of the reactants. In part d, the small circles show the total experimental cross-section.

the collisional energy transfer [29]. The sum is over the ro-vibrational states of the reactant ion, having energies $E_i$ and populations $g_i$ (where $\sum g_i = 1$). The vibrational frequencies of the complexes determined at an MP2/aug-cc-pVDZ level of theory are provided by Feller et al. [14,15]. The Beyer–Swinehart algorithm [32–35] is used to calculate the distribution of internal states of the complex at 300 K, the temperature of the gas in the flow tube.

In order to analyze the kinetic energy dependence of these cross-sections and acquire accurate thermochemistry, several effects have to be considered. First, the internal energy of the reactants must be well characterized. This is achieved by use of the flow tube ion source, yielding internal energy distributions that should be Maxwellian. As mentioned above, the cross-sections at 0 eV collision energy have finite values for a couple of the reactions studied here. This implies that some ions have internal energies greater than the dissociation threshold. In the analysis of the data, such ions are assumed to have dissociated prior to reaching the collision cell. Second, the collision

gas must provide efficient kinetic to internal energy transfer. Using Xe gas, which is heavy and polarizable while having no internal modes to carry away energy, satisfies this condition [10,30]. Third, rigorous single collision conditions are required to avoid problems associated with depositing excess (and unknown) energy in secondary collisions. To produce rigorous single collision conditions, data obtained at different neutral reactant pressures (∼0.05, 0.1, 0.2 mTorr) are extrapolated to zero pressure by linear regression [36]. These are the cross-sections shown in Figs. 1 and 2.

Fourth, because the ions move through the apparatus in a finite time ($\sim 5 \times 10^{-4}$ s), it is important to consider the lifetime of dissociating ions, particularly for large complexes, such as $Ag^+(L)_3$ or $Ag^+(L)_4$. The lifetime effect is taken into account using Rice–Ramsperger–Kassel–Marcus (RRKM) theory [37–39] in the phase space limit (PSL) using equations developed by Rodgers et al. [40]. Briefly, the transition state (TS) for dissociation is modeled by loosely interacting products such that both fragments are free to rotate. This PSL is appropriate for ion–molecule complexes because the transition state for the reverse, barrierless association process is accurately described as lying at the top of the centrifugal barrier. In this study, the two-dimensional (2-D) external rotations are treated adiabatically but with centrifugal effects included, consistent with the discussion of Waage and Rabinovitch [41]. The adiabatic 2-D rotational energy is treated using a statistical distribution with explicit summation over the possible values of the rotational quantum number, as described in detail elsewhere [40]. In the original formulation of Rodgers et al. [40], the average unimolecular dissociation rate constant for a statistical distribution of rotational quantum numbers for the adiabatic 2-D rotational energy was determined, a procedure we refer to here as the average rate constant model. Later, in treatments for multichannel dissociations, Rodgers and Armentrout [42] developed equations in which the entire dissociation probability is averaged over this statistical distribution of rotational quantum numbers, and DeTuri and Ervin [43] later pointed out that this treatment is also probably more precise for single channel CID processes. We refer to this as the average dissociation probability model here. Details of the differences between these models are provided elsewhere [43,44]. Briefly, the average dissociation probability model provides slightly lower thresholds (between 0.0 and 0.09 eV) with the difference increasing for larger complexes, a consequence of larger kinetic shifts. This is because the dissociation probability drops rapidly with increasing rotational energy of the complex (because the centrifugal barrier is higher) such that the average dissociation probability is lower than the dissociation probability calculated for the average total rate constant. The average shift for all eight systems examined was $0.03 \pm 0.03$ eV.

Data were analyzed using both a constant experimental time window available for dissociation in our instrument (noted above) and a kinetic energy-dependent time window [45]. The short limit of the time window is provided by ions that preserve their initial kinetic energy after collision (deposit no energy). The long limit is provided by ions that move with the CM velocity after collision (deposit all their available kinetic energy into internal degrees of freedom). In the present systems, the different time window treatments lead to negligible differences in the thresholds, less than 0.01 eV for all eight systems examined here. In addition, we included the possibility that the long range potential associated with the transition state for dissociation should include a term for the permanent dipole moment of the ligands studied here, as described elsewhere [44]. As shown in Table 1, this provides a systematic increase in the thresholds (because the centrifugal barrier is lower leading to more efficient dissociation and smaller kinetic shifts) of between 0.01 and 0.03 eV, with an average of $0.02 \pm 0.01$ eV for all eight systems examined. Finally, we considered whether to treat the torsional motions associated with rotations of ligands around the metal–ligand bond as vibrations or rotations. Results for these two treatments are also included in Table 1. The treatment of torsions as rotors has a somewhat different effect for each system leading to increases in the threshold energies as large as 0.03 eV or decreases as large as 0.09 eV. The

Table 1
Parameters of Eq. (3) used to model data[a]

| Complex | $\sigma_0$[b] | $N$[b] | $E_0$ (eV) (no RRKM) | $E_0$ (eV)[b] (average rate constant) | $E_0$ (eV) (average dissociation probability, no dipole, vibrators)[c] | $E_0$ (eV) (average dissociation probability, dipole, vibrators)[c] | $E_0$ (eV) (average dissociation probability, dipole, rotors)[c] |
|---|---|---|---|---|---|---|---|
| $Ag^+(H_2O)$ | 12.9 (0.9) | 0.8 (0.2) | 1.36 (0.08) | 1.36 (0.08) | 1.33 (0.08) | 1.36 (0.08) | 1.36 (0.08) |
| $Ag^+(H_2O)_2$ | 40.0 (2.6) | 0.7 (0.2) | 1.31 (0.08) | 1.31 (0.08) | 1.28 (0.08) | 1.31 (0.08) | 1.30 (0.08) |
| $Ag^+(H_2O)_3$ | 83.2 (6.7) | 0.7 (0.2) | 0.69 (0.08) | 0.66 (0.07) | 0.65 (0.07) | 0.67 (0.07) | 0.61 (0.07) |
| $Ag^+(H_2O)_4$ | 103 (4) | 0.8 (0.2) | 0.59 (0.07) | 0.58 (0.07) | 0.49 (0.07) | 0.51 (0.07) | 0.48 (0.07) |
| $Ag^+$(DME) | 20.1 (1.7) | 1.1 (0.2) | 1.51 (0.08) | 1.51 (0.08) | 1.50 (0.08) | 1.51 (0.08) | 1.51 (0.08) |
| $Ag^+(DME)_2$ | 71.6 (4.9) | 0.7 (0.2) | 1.57 (0.09) | 1.48 (0.07) | 1.47 (0.07) | 1.49 (0.07) | 1.47 (0.07) |
| $Ag^+(DME)_3$ | 114 (9) | 0.7 (0.2) | 0.84 (0.08) | 0.75 (0.08) | 0.72 (0.08) | 0.73 (0.08) | 0.62 (0.08) |
| $Ag^+(DME)_4$ | 242 (19) | 0.8 (0.1) | 0.85 (0.13) | 0.41 (0.08) | 0.40 (0.08) | 0.40 (0.08) | 0.43 (0.08) |

[a] Uncertainties are listed in parentheses.
[b] Values for average rate constant models.
[c] Silver–ligand torsions treated as vibrators or rotors.

average shift for all eight systems examined was a decrease of 0.03 ± 0.04 eV. In a previous study of $K^+(NH_3)_n$, $n = 1$–5 [44], the best agreement with literature values was obtained by using the average dissociation probability model, treating the torsions as rotors, and effects of the dipole were indeterminate. Similarly, the present system conceivably allows an evaluation of which of these various models provides thresholds agreeing with the literature most favorably. On average, the various models do not change the overall agreement with either the experimental or theoretical literature values by more than 0.05 eV. Hence, our final results are reported as those using the average dissociation probability model and the dipole moment included in the long range potential. The choice of how to treat torsions is more complicated and addressed further below. The only systems that are particularly sensitive to the specific treatment are $Ag^+(H_2O)_4$ and $Ag^+(DME)_3$, and in both cases changes in the thresholds for any treatment still lie within the uncertainties quoted in the final number.

Because the rotational, vibrational, and translational energy distributions are explicitly included in our modeling, the threshold energies determined with Eq. (3) correspond to 0 K. By assuming that $E_0$ represents the energy difference between the reactants and products at 0 K [10], threshold energies for CID reactions are equated with 0 K bond dissociation energies (BDEs). This correspondence is generally true for ion–molecule reactions because the presence of activation barriers in excess of the reaction endothermicity is unlikely [46–49], especially for the simple heterolytic bond cleavages considered here [50]. The reported thresholds for all reactions are determined in the following way. First, Eq. (3) with an initial set of parameters is convoluted with the kinetic energy distribution of the ion beam and the thermal motion of Xe gas in the reaction cell. The parameters of Eq. (3) are optimized using a nonlinear least-squares analysis to give a best fit to the zero pressure extrapolated cross-sections. This represents the threshold energy at 0 K without lifetime corrections. The threshold energies, including the PSL analysis, provide the bond energy at 0 K, including lifetime corrections. An estimate of the absolute uncertainty in the threshold energy is obtained by variations in the parameter $N$ in Eq. (3), variations in the time available for reaction by factors of 2 and 1/2, variations in the vibrational frequencies of the reactant and transition state by ±10%, and the error in the absolute energy scale (±0.05 eV lab). Threshold energies along with the optimum fitting parameters, $\sigma_0$ and $N$, for all eight systems studied here are listed in Table 1.

To allow comparison to previous literature values and commonly used experimental conditions, we convert the 0 K bond energies determined here to 298 K bond enthalpies and free energies. The enthalpies and entropy conversions are calculated using standard formulas and the vibrational and rotational constants determined at the MP2/aug-cc-pVDZ level [14,15]. Table 2 lists 0 and 298 K enthalpies, enthalpic and entropic corrections for all systems experimentally determined. Here, the choice of whether torsions are treated as vibrators or rotors can make an appreciable difference, so values for both treatments are listed. These conversions are performed self-consistently in that data analyzed to yield $\Delta H_0$ values with torsions treated as vibrators or rotors (listed in Table 1) are converted to 298 K values making the same assumption. Uncertainties in the conversion values are determined by increasing and decreasing frequencies of the ligands by 10% and the metal–ligand frequencies by a factor of 2. For comparison to literature values, we take the average of the two treatments with error bars expanded to include the differences between the two values. These are reported in Table 3.

Once the 298 K values are determined, we find one interesting observation that involves the Gibbs free energies, $\Delta G_{298}$, for $Ag^+(H_2O)_4$. Because the ground state structure of this complex (designated $3 + 1$) is calculated to have one ligand in the second solvent shell (see Section 4 below), the entropy change for dissociation is large and leads to negative values for $\Delta G_{298}$ for both treatments of the torsions. However, if we assume that our source generates a low-lying conformer in which all four ligands are in the first solvent shell ($4 + 0$), then the calculated $\Delta G_{298}$ value is small but positive. Thus, it is possible

Table 2
Enthalpies and free energies for $Ag^+(H_2O)_n$ and $Ag^+(DME)_n$ at 0 and 298 K (in kJ/mol)

| Complex | $\Delta H_0$[a] | $\Delta H_{298} - \Delta H_0$[b] | $\Delta H_{298}$ | $T\Delta S_{298}$[b] | $\Delta G_{298}$ |
|---|---|---|---|---|---|
| $Ag^+(H_2O)$[c] | 131 ± 8 | 2.8 ± 2.0 | 134 ± 8 | 26 ± 5 | 109 ± 9 |
| $Ag^+(H_2O)_2$ | 126 ± 8 | 0.3 ± 1.1 | 127 ± 8 | 34 ± 6 | 93 ± 10 |
| | *125 ± 8* | *1.2 ± 1.1* | *127 ± 8* | *33 ± 6* | *94 ± 10* |
| $Ag^+(H_2O)_3$ | 65 ± 7 | 0.0 ± 1.1 | 65 ± 7 | 26 ± 6 | 39 ± 9 |
| | *59 ± 7* | *2.4 ± 1.1* | *61 ± 7* | *16 ± 6* | *45 ± 9* |
| $Ag^+(H_2O)_4$ (3 + 1) | 49 ± 10 | 4.8 ± 1.4 | 54 ± 10 | 69 ± 6 | −15 ± 12 |
| | *46 ± 10* | *2.5 ± 1.4* | *49 ± 10* | *75 ± 6* | *−26 ± 12* |
| $Ag^+(H_2O)_4$ (4 + 0) | 49 ± 10 | −1.8 ± 1.4 | 47 ± 10 | 46 ± 6 | 1 ± 12 |
| | *46 ± 10* | *−0.7 ± 1.4* | *46 ± 10* | *37 ± 6* | *8 ± 12* |
| $Ag^+(DME)$[c] | 146 ± 8 | 0.9 ± 1.4 | 147 ± 8 | 28 ± 5 | 119 ± 9 |
| $Ag^+(DME)_2$ | 144 ± 7 | −1.4 ± 1.3 | 142 ± 8 | 41 ± 7 | 101 ± 11 |
| | *142 ± 7* | *−0.4 ± 1.3* | *141 ± 8* | *38 ± 7* | *103 ± 11* |
| $Ag^+(DME)_3$ | 70 ± 13 | −3.0 ± 0.7 | 67 ± 13 | 36 ± 6 | 31 ± 14 |
| | *60 ± 13* | *−0.8 ± 0.7* | *59 ± 13* | *22 ± 6* | *37 ± 14* |
| $Ag^+(DME)_4$ | 39 ± 8 | −6.8 ± 0.9 | 32 ± 8 | 13 ± 6 | 19 ± 10 |
| | *42 ± 8* | *−5.4 ± 0.9* | *36 ± 8* | *14 ± 6* | *22 ± 10* |

[a] Values taken from Table 1 using the average dissociation probability model and including the dipole potential. Values in roman treat torsions as vibrations, whereas values in italics treat torsions as rotations.
[b] Calculated using standard formulas and molecular constants determined at the MP2/aug-cc-pVDZ level of theory [14,15]. Uncertainties correspond to changes in the metal–ligand frequencies by a factor of 2 and ±10% vibrations in the $H_2O$ and DME vibrational frequencies.
[c] Values for both treatments of the torsions are identical.

that in the room temperature flow tube, generation of $Ag^+(H_2O)_4$ forms the 4 + 0 structure rather than the 3 + 1 structure that is the 0 K ground state. This possibility is discussed further below.

### 3.3. Experimental and theoretical BDEs

#### 3.3.1. $Ag^+(H_2O)_n$

The 298 K BDEs for $Ag^+(H_2O)_n$ measured experimentally are 134 ± 8 kJ/mol, 127 ± 8 kJ/mol, 63 ± 9 kJ/mol, and 51 ± 12 kJ/mol (47 ± 11 if the 4 + 0 structure is assumed) for $n$ = 1–4, respectively. Strong BDEs are observed for the first and second $H_2O$ ligands with the second BDE slightly weaker than the first. The third and fourth $H_2O$ ligands bind much more weakly than the first and second ligands. Comparison of these experimental BDEs for $Ag^+(H_2O)_{n-1}$–$H_2O$ with the theoretical values of Feller et al. [14] and previous experimental results [12,17] are given in Table 3. Just as in our results, the strong BDEs for $n$ = 1 and 2 and substantially weaker BDEs for $n$ = 3 and 4 are reported in all literature values. Our experimental values are in reasonable agreement with the $Ag^+H_2O$ BDE reported by Siu and coworkers [17] obtained using TCID techniques and with the values obtained by Holland and Castleman [12] using high pressure mass spectrometry techniques (HPMS). The mean absolute deviation (MAD) between our TCID and the HPMS experimental results is 9 ± 9 kJ/mol, comparable to our experimental uncertainties. Clearly, our value for $Ag^+(H_2O)_4$ obtained by assuming the 3 + 1 structure agrees better with the HPMS value. (It might be noted that the HPMS results for the strongly bound $Ag^+(H_2O)$ and $Ag^+(H_2O)_2$ complexes were obtained at relatively high temperatures, between 500 and 700 K. If corrections for the change in dissociation enthalpy as a function of temperature are estimated using the theoretical molecular parameters, we estimate that the 298 K dissociation enthalpies for these two complexes are 140 and 110 kJ/mol, rather than the 139 and 106 kJ/mol reported. Clearly such small corrections were justifiably ignored in the original treatment, but this does demonstrate that the absolute uncertainty in the latter value is probably higher than the reported ±1 kJ/mol. For $Ag^+(H_2O)_3$ and

Table 3
298 K bond dissociation energies for $M^+(L)_n$ complexes, where L = $H_2O$ and DME and $M^+$ = $Ag^+$, $Cu^+$, $K^+$, and $Na^+$

| Complex | $Ag^+$ | | | $Cu^+$ | | $K^+$ | | $Na^+$ | |
|---|---|---|---|---|---|---|---|---|---|
| | Experimental (this work) | Experimental (literature) | Theory | Experimental | Theory | Experimental | Theory | Experimental | Theory |
| $M^+(H_2O)$ | 134 ± 8[a] | 139 ± 9[b] (140), 135 ± 11[g] | 133[c] | 161 ± 8[d] | 163[c] | 75[e] | 77[f] | 100[e] | 99[f] |
| $M^+(H_2O)_2$ | 127 ± 8[a] | 106 ± 1[b] (110) | 117[c] (118) | 170 ± 7[d] | 183[c] | 67[e] | 65[f] | 83[e] | 83[f] |
| $M^+(H_2O)_3$ | 63 ± 9[a] | 63 ± 1[b] | 52[c] (55) | 57 ± 8[d] | 69[c] | 55[e] | 57[f] | 66[e] | 69[f] |
| $M^+(H_2O)_4$ | | 62 ± 1[b] | | 54 ± 4[d] | 63[c] | 49[e] | 48[f] | 58[e] | 53[f] |
| (3 + 1) | 51 ± 12[a] | | 56[c] (58) | | | | | | |
| (4 + 0) | 47 ± 11[a] | | 43[c] (45) | | | | | | |
| $M^+$(DME) | 147 ± 8[a] | | 154[h,i] | 186 ± 12[j,k] | 204[h,k] | 74 ± 4[l] | 79[l] | 93 ± 5[m] | 108[m] |
| $M^+(DME)_2$ | 142 ± 8[a] | | 152[h,i] | 191 ± 8[j,k] | 210[h,k] | 65 ± 4[l] | 64[l] | 79 ± 5[m] | 90[m] |
| $M^+(DME)_3$ | 63 ± 17[a] | | 65[h,i] | 51 ± 4[j,k] | 54[h,k] | 53 ± 7[l] | 58[l] | 67 ± 5[m] | 71[m] |
| $M^+(DME)_4$ | 34 ± 10[a] | | 59[h,i] | 42 ± 10[j,k] | 45[h,k] | 46 ± 8[l] | 55[l] | 58 ± 4[m] | 57[m] |

[a] This work, average of $\Delta H_{298}$ values from Table 2.
[b] Ref. [12]. Values in parentheses have been adjusted to 298 K as described in the text.
[c] Ref. [14]. Values in parentheses have been adjusted to 298 K using data in Table 2.
[d] Ref. [10].
[e] Ref. [22].
[f] Ref. [52].
[g] Ref. [17].
[h] Ref. [15].
[i] Adjusted from 0 K values using data in Table 2.
[j] Ref. [11].
[k] Adjusted from 0 K values calculated using standard formulas and vibrational frequencies determined at the HF/6-31+G* level of theory and scaled by 0.8929.
[l] Ref. [7].
[m] Ref. [6].

$Ag^+(H_2O)_4$ complexes, the HPMS measurements are obtained near room temperature so no thermal corrections are required.)

Interestingly, the theoretical BDE for $Ag^+(H_2O)$–$H_2O$ determined by Feller et al. [14] using a complete basis set extrapolation protocol lies exactly in the middle of the two experimental values, lying just at the border of our experimental uncertainty. The theoretical BDEs of Feller et al. are also in good agreement with our values for the other sized complexes. Slightly better agreement is obtained if the thermal corrections listed in Table 2 are used for both experimental and theoretical values. Unfortunately, comparison with theory does not resolve which structure for $Ag^+(H_2O)_4$ is most likely present in our experiment as the results are consistent with either, although slightly better agreement is obtained for the 4 + 0 structure. The MAD between our experimental and the theoretical results (for both possible structures of $Ag^+(H_2O)_4$) is 6 ± 4 kJ/mol for $n$ = 1–4, compared to 8 ± 3 kJ/mol for the HPMS numbers and theory (using the 3 + 1 structure).

### 3.3.2. $Ag^+(DME)_n$

The 298 K BDEs for $Ag^+(DME)_n$ measured experimentally are 147 ± 8 kJ/mol, 142 ± 8 kJ/mol, 63 ± 17 kJ/mol, and 34 ± 10 kJ/mol for $n$ = 1–4, respectively. As for $Ag^+(H_2O)_n$ complexes, strong BDEs are observed for the first and second DMEs with the second BDE somewhat weaker than the first. Both experimental and theoretical BDEs are weaker for the third and fourth DME ligands than the first and second ligands. The BDEs for DME are slightly larger than those for $H_2O$ except for the fourth DME, which binds significantly more weakly than the fourth $H_2O$. Our experimental values are in reasonable agreement with

theoretical values [15] with the exception of $n = 4$. The average deviation between the experimental and MP2 theoretical results is $11 \pm 10$ kJ/mol for $n = 1$–4 ($6 \pm 4$ kJ/mol for $n = 1$–3), essentially within our experimental uncertainty.

A large deviation between theory and experiment is found for the $Ag^+(DME)_4$ complex. Hence, we reproduced these experimental results using two different instruments to be sure that there were no experimental artifacts. As discussed above, to ensure that our analysis of the data was complete in this case, we tried alternate analysis treatments including different treatments of the time window available for dissociation, vibrational frequencies as vibrators and rotors, excluding and including the dipole moment in the long range potential, and the average rate constant and dissociation probability models. The value that we believe includes all possible effects, and therefore reported in Table 3, also leads to the largest threshold obtained (Table 1). We also tried fitting both the total cross-section and the cross-section for the primary $Ag^+(DME)_3$ product in which the subsequent decay by loss of an additional DME ligand was included using a procedure detailed elsewhere [51]. The high energy decay utilized parameters similar to those previously obtained for the analysis of the $K^+(DME)_4$ complex [7]. Very similar thresholds were obtained from the analysis of the total and individual product cross-sections. We note that the kinetic shift in the $Ag^+(DME)_4$ system is much larger than for other complexes studied here, such that it is possible that the kinetic shift is overestimated in this system. However, the PSL transition state is the loosest transition state that is physically realistic, which should lead to the smallest kinetic shift, so we can see no means of realistically reinterpreting the data to decrease the kinetic shift and thereby increase the BDE. In that regard, we verified that reinterpretation of our data for the $K^+(DME)_4$ yielded the published bond energy [7] and also discovered that the data for the silver and potassium systems are nearly identical. The differences in thresholds observed are attributable almost entirely to differences in the lowest frequency vibrations of the $M^+(DME)_3$ product used as the transition state in the kinetic shift modeling. The only other possible explanation for a low experimental bond energy in this system is that the ground state $Ag^+(DME)_4$ complex has not been formed, but it is unclear why this would be the case for the $Ag^+(DME)_4$ complex and for no other $M^+(DME)_4$ complex we have studied.

## 4. Discussion

Experimental and theoretical BDEs for $Ag^+(H_2O)_n$ and $Ag^+(DME)_n$ are listed in Table 3 along with values for analogous complexes of other metal ions [6,7,10–12,14,15,17,22,52]. The theoretical structures of the complexes considered here are shown in Fig. 3 and taken from Refs. [14,15]. The main attractive forces between the ligand and any of the metal cations are ion–dipole and ion-induced dipole interactions, which have $r^{-2}$ and $r^{-4}$ dependences, respectively. Dipole moments of $H_2O$ and DME are 1.84 and 1.30 D, respectively, whereas their polarizabilities are 1.45 and 5.24 $Å^3$, respectively [53–55]. Previous work [11] on $Cu^+$ complexes shows that DME binds more strongly than $H_2O$ because of the larger polarizability of DME. Similarly, DME binds more strongly to $Ag^+$ ion than $H_2O$ for $n = 1$–3, as indicated by both experiment and theory. Note that the BDEs of $Ag^+$ to one $H_2O$ and DME ligand are smaller than those to the $Cu^+$ ion by about 20%. These differences can be explained by the increase in the metal ion size. Because copper has a smaller ionic radius (0.96 Å) than silver (1.26 Å), the copper ion complexes have shorter M–O bond lengths than the corresponding silver ion complexes and stronger electrostatic interactions.

However, comparison of the BDEs of $Ag^+$ with those of $K^+$, which has a similar ionic radius of 1.33 Å, demonstrates that effects besides metal ion size must also be active (see Table 3 and Fig. 4). For instance, the BDEs of $K^+$ to $H_2O$ and DME are almost identical. This difference can be explained because the $Ag^+$ ion complexes have shorter metal–ligand bond lengths, which allows the highly polarizable DME ligand to bind more strongly. However, the most dramatic difference lies in the BDEs of the first two ligands, which are almost twice as strong for $Ag^+$ as for $K^+$. The $Ag^+$

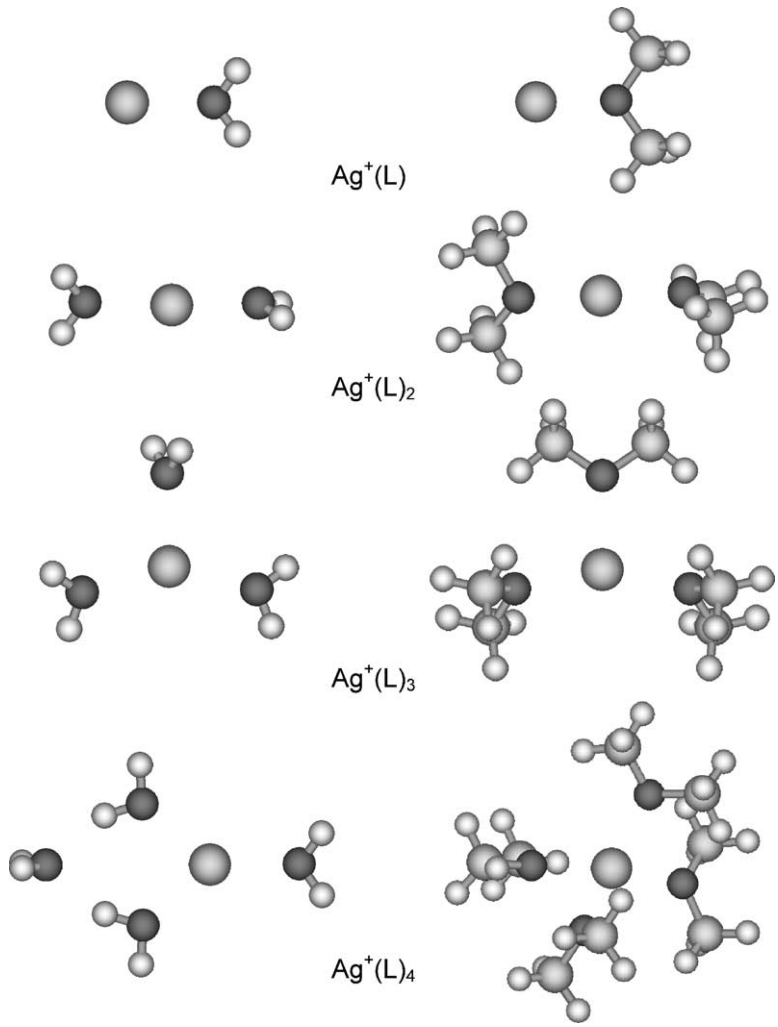


Fig. 3. Structures of the $Ag^+(L)_n$ ($n = 1$–4) systems where L = $H_2O$ (left side) and DME (right side) taken from theoretical calculations [14,15].

ion has a $^1S$ ($5s^04d^{10}$) ground state electronic configuration, whereas $K^+$ has a $^1S$ ($4s^03d^0$) configuration, such that the fully occupied d shell is the main distinction between the two metal ions. It has been shown that the coinage ions can bind one and two ligands more strongly than alkali metal ions that have a similar ionic radius as a result of s-dσ hybridization [13]. Briefly, as the first ligand approaches a coinage metal cation, the doubly occupied valence dσ orbital hybridizes with the empty valence s orbital. The s-dσ hybrid localized along the bonding axis is left empty to act as an acceptor orbital for electron density from the ligand. The pair of electrons originally in the dσ orbital occupies the s-dσ orbital localized perpendicular to the bonding axis. Thus, hybridization reduces the electron density of the metal along the bonding axis, thereby reducing metal–ligand repulsion and increasing the effective nuclear charge seen by the ligand. Thus, the BDE is much stronger than the corresponding BDE found for the alkali metal ion having a similar ionic metal radius.

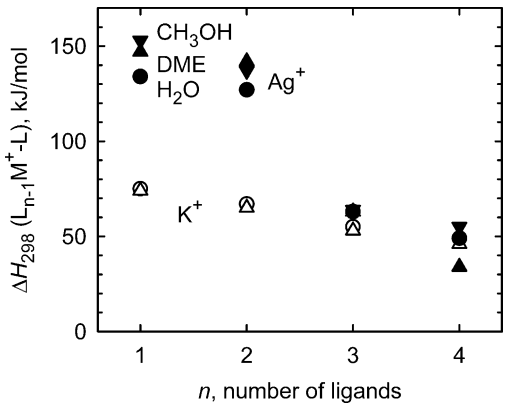


Fig. 4. Sequential bond energies (in kJ/mol) for water (circles), methanol (inverted triangles), and dimethyl ether (triangles) bound to silver ion (solid symbols) and potassium ion (open symbols). Data are taken from Table 3 except for the methanol systems [21].

Because of the symmetry of the s-dσ hybrid orbitals, a second ligand, located 180° away from the first, can donate electrons to the same empty s-dσ hybrid orbital. Thus, the second ligand also feels less repulsion and a higher nuclear charge, while the energetic cost of hybridization is shared by two ligands. Hence, the BDE of the second ligand is comparable to that of the first, in contrast to BDEs for the analogous alkali metal ion complexes where the second ligand binds less strongly than the first ligand. Such arguments are supported by previous experimental observations [10,11] and by the results for $Ag^+$ and $K^+$ shown in Table 3 and Fig. 4.

In the case of $Cu^+$, the BDEs of the second water and DME ligands to the metal ion are stronger than those of the first ligand [10,11], consistent with strong 4s-3dσ hybridization. However, for the $Ag^+$ ion, the second ligand (DME, $H_2O$, methanol) binds more weakly than the first. The effect of 5s-4dσ hybridization is expected to be smaller than that of 4s-3dσ hybridization because the ionic radius of the metal ion increases. In addition, the hybridization of $Ag^+$ becomes less effective than that of $Cu^+$ because the d-s hybridization energy, which scales with the energy needed to excite from the ground state $d^{10}$ configuration to the $s^1d^9$ configuration, is 4.86 eV for $Ag^+$, much higher than that for $Cu^+$ (2.72 eV) [56].

Because of the symmetry of the s-dσ hybrid orbitals, the enhancement in BDEs is most effective for two ligands. A third ligand is forced to interact with the electron density in the occupied s-dσ hybrid such that this bond energy is much weaker than the first two. The BDEs for the third water and DME are slightly stronger to the $Ag^+$ ion than to $K^+$ (about 17% or 9 kJ/mol). The small increase may be attributed to some residual 5s-4dσ hybridization, which is evidenced by O–$Ag^+$–O bond angles of 149.0 and 155.7° between two tightly bound $H_2O$ and DME ligands, respectively [57], compared with the 120° bond angle found in the analogous $K^+$ complexes [52]. In the $Ag^+(H_2O)_3$ and $Ag^+(DME)_3$ complexes, the two tightly bound ligands have Ag–O bond lengths that are shorter (2.242 and 2.192 Å, respectively) than those of the loosely bound third ligands (2.305 and 2.284 Å, respectively).

Theoretical studies by Feller et al. show that all three $H_2O$ and DME ligands in the $Ag^+(L)_3$ complexes bind directly to the $Ag^+$ ion [14,15]. This is different from the $Cu^+(H_2O)_3$ system which has a ground state conformer with two $H_2O$ molecules attached directly to the $Cu^+$ ion [14]. Here, the third ligand forms a hydrogen bond with one of the water ligands in the first solvation shell, which are strongly polarized because of the positive charge on $Cu^+$ cation. Apparently, the third $H_2O$ in the $Ag^+(H_2O)_3$ complex does not engage in such strong hydrogen bonding because of the larger ionic radius, reducing the polarization of the first two $H_2O$ ligands. The DME ligands cannot engage easily in hydrogen bonding, hence, the third and fourth DMEs attach directly to the metal ion for both $Cu^+$ and $Ag^+$. This difference in geometries results in a BDE for the third water to the $Cu^+$ ion that is slightly larger than that of the DME ligand. Interestingly, the BDEs of the third $H_2O$ and DME ligands to $Ag^+$ ion are larger than the corresponding BDEs in $Cu^+$ complexes, in contrast to the BDEs for the first two ligands. In essence, the explanation is the same because the third ligand disrupts the more effective 4s-3dσ hybridization in the $Cu^+(L)_3$ ion complexes, leading to a weaker bond than in the silver complexes. Equivalently, this can be understood by realizing that

the average bond energy for loss of all three ligands from $Cu^+(L)_3$ remains larger than that for $Ag^+(L)_3$, as expected for the smaller ion, but the third ligand bond is weak for $Cu^+$ because the first two BDEs are so much larger.

For $n = 1$–3, the BDEs of DME to $Ag^+$ are very similar to those measured for methanol (MeOH) to $Ag^+$ (Fig. 4) [21]. However, for $n = 4$, our experimental results find that both $H_2O$ and MeOH bind to $Ag^+$ more strongly than DME, whereas theory finds comparable bond energies for all three ligand systems (Table 3 and Ref. [21]). The theoretical studies show that the fourth $H_2O$ binds by hydrogen bonds to two of the $H_2O$ ligands bound directly to the $Ag^+$ ion [14]. This geometry allows some residual s-dσ hybridization to be retained in the $Ag^+(H_2O)_4$ complex. (Note that this constrained geometry leads to a large entropy change upon dissociation of this complex, Table 2.) In the calculations, the structure in which all four ligands bind directly to $Ag^+$ lies 13 kJ/mol higher in energy. In the $Ag^+(MeOH)_4$ complex [21], all four ligands bind to the metal, but there is a weak hydrogen bond between two of the ligands, enhancing its stability. However, no hydrogen bonding structures are available for the analogous DME complex because there are no acidic protons in DME. The fourth DME ligand in coinage ion complexes binds weakly because these complexes lose the $(n + 1)$s-$n$dσ hybridization completely. This is shown by the formation of symmetric $S_4$ structures for both $Ag^+(DME)_4$ and $Cu^+(DME)_4$ complexes [15].

## 5. Conclusion

Kinetic energy-dependent CID in a guided ion beam tandem mass spectrometer is used to determine the absolute bond energies of $Ag^+(H_2O)_n$ and $Ag^+(DME)_n$ for $n = 1$–4. Effects of multiple collisions, internal energies of the complexes, reactant translational energy distributions, and dissociation lifetimes are all considered in the analysis of the experiments. Our experimental results show strong BDEs for $n = 1$ and 2, decreasing slightly for $n = 2$, and much weaker BDEs for $n = 3$ and 4. Our experimental BDEs for $Ag^+(H_2O)_n$ complexes are in good agreement with previous experimental results [12,17] and these along with results for the DME complexes agree nicely with theoretical results [14,15] except for $Ag^+(DME)_4$, where the experimental result appears low.

The overall trends in the absolute BDEs can be explained by 5s-4dσ hybridization, which removes electron density along the bonding axis for two ligands at 180°. In contrast to the trend observed for the silver ion complexes, the second ligand binds more strongly than the first for the analogous complexes of $Cu^+$. The difference is easily rationalized by the increase in metal ionic radius and larger d-s excitation energy for $Ag^+$, which reduces the effectiveness of the s-dσ hybridization. For $n = 1$–3, DME binds more strongly to a silver ion than $H_2O$ does because of its larger polarizability. For $n = 4$, DME binds more weakly than $H_2O$ because the fourth $H_2O$ can engage in hydrogen bonding to two of the inner shell ligands and thereby retain some favorable 5s-4dσ hybridization, whereas DME cannot.

## Acknowledgements

This work is supported by the National Science Foundation, CHE-0135517. The authors thank Dr. D. Feller for providing the frequencies, structures, and 0 K bond enthalpies for the complexes studied here.

## References

[1] G.L. Eichhorn, Adv. Inorg. Biochem. 3 (1981) 1.
[2] E.P. Horwitz, M.L. Dietz, D.E. Fisher, Solvent Extr. Ion Exch. 9 (1991) 1.
[3] J.W. Grate, R. Strebin, J. Janata, O. Egorov, J. Ruzicka, J. Anal. Chem. 68 (1996) 333.
[4] D. Ray, D. Feller, M.B. More, E.D. Glendening, P.B. Armentrout, J. Phys. Chem. 100 (1996) 1605.
[5] D. Ray, D. Feller, M.B. More, E.D. Glendening, P.B. Armentrout, J. Phys. Chem. 100 (1996) 16116.
[6] M.B. More, D. Ray, P.B. Armentrout, J. Phys. Chem. A 101 (1997) 831.

[7] M.B. More, D. Ray, P.B. Armentrout, J. Phys. Chem. A 101 (1997) 4254.
[8] M.B. More, D. Ray, P.B. Armentrout, J. Phys. Chem. A 101 (1997) 7007.
[9] N.F. Dalleska, B.L. Tjelta, P.B. Armentrout, J. Phys. Chem. 98 (1994) 4191.
[10] N.F. Dalleska, K. Honma, L.S. Sunderlin, P.B. Armentrout, J. Am. Chem. Soc. 116 (1994) 3519.
[11] H. Koizumi, X.G. Zhang, P.B. Armentrout, J. Phys. Chem. A. 105 (2001) 2444.
[12] P.M. Holland, A.W. Castleman, J. Chem. Phys. 76 (1982) 4195.
[13] C.W. Bauschlicher, S.R. Langhoff, H. Partridge, J. Chem. Phys. 94 (1991) 2068.
[14] D. Feller, E.D. Glendening, W.A. de Jong, J. Chem. Phys. 110 (1999) 1475.
[15] D. Feller, D.A. Dixon, J. Phys. Chem. A 106 (2002) 5136.
[16] H. Deng, P. Kebarle, J. Phys. Chem. A 102 (1998) 571.
[17] H.E. Aribi, T. Shoeib, Y. Ling, C.F. Rodriquez, A.C. Hopkinson, K.W.M. Siu, J. Phys. Chem. A 99 (1995) 3060.
[18] T. Shoeib, H.E. Aribi, K.W.M. Siu, A.C. Hopkinson, J. Phys. Chem. A 105 (2001) 710.
[19] Y.M. Chen, P.B. Armentrout, Chem. Phys. Lett. 210 (1993) 123.
[20] F. Meyer, Y.M. Chen, P.B. Armentrout, J. Am. Chem. Soc. 117 (1995) 4071.
[21] H. Koizumi, M. Larsen, P.B. Armentrout, D. Feller, J. Phys. Chem. A 107 (2003) 2329.
[22] I. Dzidic, P. Kebarle, J. Chem. Phys. 74 (1970) 1466.
[23] K.M. Ervin, P.B. Armentrout, J. Chem. Phys. 83 (1985) 166.
[24] R.H. Schultz, P.B. Armentrout, Int. J. Mass Spectrom. Ion Processes 107 (1991) 29.
[25] R.H. Schultz, P.B. Armentrout, J. Chem. Phys. 96 (1992) 1046.
[26] R.H. Schultz, K.C. Crellin, P.B. Armentrout, J. Am. Chem. Soc. 113 (1991) 8590.
[27] F.A. Khan, D.C. Clemmer, R.H. Schultz, P.B. Armentrout, J. Phys. Chem. 97 (1993) 7978.
[28] D. Gerlich, in: State-Selected and State-to-State Ion-Molecule Reaction Dynamics, Part 1, Experiment, in: C.Y. Ng, M. Baer (Eds.), Advances in Chemical Physics Series, vol. LXXXII, Wiley, New York, 1992, p. 1.
[29] F. Muntean, P.B. Armentrout, J. Chem. Phys. 115 (2001) 1213.
[30] N. Aristov, P.B. Armentrout, J. Phys. Chem. 90 (1986) 5135.
[31] S.K. Loh, D.A. Hales, L. Lian, P.B. Armentrout, J. Chem. Phys. 90 (1989) 5466.
[32] T.S. Beyer, D.F. Swinehart, Commun. Assoc. Comput. Machinery 16 (1973) 379.
[33] S.E. Stein, B.S. Rabinovitch, J. Chem. Phys. 58 (1973) 2438.
[34] S.E. Stein, B.S. Rabinovitch, Chem. Phys. Lett. 49 (1977) 183.
[35] R.G. Gilbert, S.C. Smith, Theory of Unimolecular and Recombination Reactions, Blackwell Scientific Publications, Oxford, 1990.
[36] D.A. Hales, L. Lian, P.B. Armentrout, Int. J. Mass Spectrom. Ion Processes 102 (1990) 269.
[37] R.A. Marcus, O.K. Rice, J. Phys. Colloid Chem. 55 (1951) 894.
[38] R.A. Marcus, J. Chem. Phys. 20 (1952) 359.
[39] H.M. Rosenstock, M.B. Wallenstein, A.L. Wahrhaftig, H. Eyring, Proc. Natl. Acad. Sci. U.S.A. 38 (1952) 667.
[40] M.T. Rodgers, K.M. Ervin, P.B. Armentrout, J. Chem. Phys. 106 (1997) 4499.
[41] E.V. Waage, B.S. Rabinovitch, Chem. Rev. 70 (1970) 377.
[42] M.T. Rodgers, P.B. Armentrout, J. Chem. Phys. 109 (1998) 1787.
[43] V.F. DeTuri, K.M. Ervin, J. Chem. Phys. A 103 (1999) 6911.
[44] C. Iceman, P.B. Armentrout, Int. J. Mass Spectrom. 222 (2002) 329.
[45] F. Muntean, L. Heumann, P.B. Armentrout, J. Chem. Phys. 116 (2002) 5593.
[46] B.H. Boo, P.B. Armentrout, J. Am. Chem. Soc. 109 (1987) 3459.
[47] K.M. Ervin, P.B. Armentrout, J. Phys. Chem. 88 (1984) 5454.
[48] P.B. Armentrout, in: P. Ausloos, S.G. Lias (Eds.), Structure/Reactivity and Thermochemistry of Ions, Reidel, Dordrecht, 1987, p. 97.
[49] P.B. Armentrout, in: N.G. Adams, L.M. Babcock (Eds.), Advances in Gas-Phase Ion Chemistry, vol. 1, JAI, Greenwich, 1992, p. 83.
[50] P.B. Armentrout, J. Simons, J. Am. Chem. Soc. 114 (1992) 8627.
[51] M.E. Weber, J.L. Elkind, P.B. Armentrout, J. Chem. Phys. 84 (1986) 1521.
[52] E.D. Glendening, D. Feller, J. Phys. Chem. 99 (1995) 3060.
[53] K.L. Ramaswarmy, Proc. Indian Acad. Sci. Sect. A. 4 (1936) 675.
[54] H.A. Stuart, Die Struktur des Freien Molekuls Springer-Verlag, Berlin, 1952, p. 441.
[55] E.W. Rothe, R.B. Bernstein, J. Chem. Phys. 31 (1959) 1619.
[56] C.E. Moore, Atomic Energy Levels, NSRDS-NBS35, Washington, DC, 1971.
[57] D. Feller, personal communication.